Available online at www.sciencedirect.com
SCIENCE DIRECT®
Solar Energy Materials & Solar Cells
ELSEVIER
Solar Energy Materials & Solar Cells 90 (2006) 1105–1120
www.elsevier.com/locate/solmat

# Analysis and modelling the reverse characteristic of photovoltaic cells

M.C. Alonso-García[a,*], J.M. Ruíz[b]

[a]*CIEMAT-DER, Av. Complutense 22, 28040 Madrid, Spain*
[b]*E.T.S.I. de Telecomunicación-UPM, Av. Complutense s/n, 28040 Madrid, Spain*

Received 22 May 2005; accepted 27 June 2005
Available online 10 August 2005

**Abstract**

Models to represent the behaviour of photovoltaic (PV) solar cells in reverse bias are reviewed, concluding with the proposal of a new model. This model comes from the study of avalanche mechanisms in PV solar cells, and counts on physically meaningful parameters. It can be adapted to PV cells in which reverse characteristic is dominated by avalanche mechanisms, and also to those dominated by shunt resistance or with breakdown voltages far from a safe measurement range. A procedure to calculate model parameters based in piece-wise fitting is also proposed. The model has been applied to isolated crystalline solar cells measured at different conditions, and also to cells encapsulated in a conventional PV module. Good fitting has been found between the experimental and modelled curves. Evolution of calculated breakdown voltages with temperature is in accordance with avalanche theories.
© 2005 Elsevier B.V. All rights reserved.

*Keywords:* Characterisation; Modelling; Reverse-bias; Hot-spot

## 1. Background

The study of photovoltaic (PV) devices working in reverse bias was significant since high voltages and abnormally high temperatures were found in spatial PV

*Corresponding author. Tel.: +34 91 346 6360; fax: +34 91 346 6037.
*E-mail address:* carmen.alonso@ciemat.es (M.C. Alonso-García).

0927-0248/$ - see front matter © 2005 Elsevier B.V. All rights reserved.
doi:10.1016/j.solmat.2005.06.006

applications [1]. From that, and with the identification of the hot-spot effect, studies were performed to analyse its consequences [2] and to evaluate its influence in series–parallel associations of PV devices [3]. In 1972 first studies focused in the analysis of reverse characteristics in PV cells and the influence of material defects in it were performed [4].

From that moment the topic became of interest, as it was related to mismatch effects, the output of a PV array in case of partial shading and the reliability of the system [5–8]. Besides, it pointed to the use of by-pass diodes [9–12] and their appropriate distribution when part of the system is shaded [11,13–18].

Nowadays current tendencies in PV with new cell designs, higher cell sizes and modules with more interconnected cells make it a key topic to guarantee long lifetime of the PV module. Besides, an increase in grid connected applications in the urban environment is being produced in the last few years [19]. These types of systems are located in many cases adapted to the characteristics of the building, with orientation and tilted angles different from the optimum, which may cause partial shading. In the last few years several works have been published in order to evaluate the influence of the reverse characteristic in the power dissipated in the cell and in the currents and temperature distributions on cell surface in case of shading [20–22]. These works in general highlight the importance of reverse bias $I$–$V$ characteristic measurements and analysis in order to determine worst case in hot-spot testing [23–26].

Finally, the measurement of reverse characteristic is also important in multi-junction solar cells and in concentration PV arrays: in the first because it can be complementary to spectral response measurements [27], and in the second because mismatch among cells has greater influence on the output due to the increase in currents produced by the concentration rate [28].

With this background, a study has been performed to supply a model for reverse biased solar cell $I$–$V$ characteristics, applicable to different types of cells in various operational conditions. First, a revision of models presented in bibliography has been performed. This led us to review avalanche theories, in order to adapt them to current solar cells, and to propose a new model. The model should be valid for the different types of reverse characteristics found, and model parameters should keep their physical meaning if possible.

## 2. Revision of solar cell models in reverse bias

There are several equations proposed in literature to simulate the behaviour of PV cells in reverse bias. Most of them come from the conventional $I$–$V$ equation in the forward region modified in some way to introduce avalanche effects. Main contributions in chronological order are summarized in the following:

- Hartman et al. [29] use the equation

$$I = \frac{[I_L(T,E) + I_D(V,T)]}{1 - \left(V/V_b\right)^n}, \tag{1}$$

where $V_b$ is the breakdown voltage, considered constant, $n$ is the Miller exponent [30] ($3<n<6$ ), $I_L$ ($T$,$E$ ) is the photocurrent, dependant on temperature and irradiance, $I_D$ ($V$,$T$ ) is the dark current.

- In 1982 Spirito and Abergamo [31] made a distinction between A-type cells, dominated in reverse bias by avalanche multiplication, and B-type cells, dominated by shunt resistance effects in reverse bias. Reverse bias equation for A-type cells is

$$I = \left(I_{sc} - I_0\left(\exp\frac{V}{mV_t} - 1\right)\right)M(V) \text{ with } M = \frac{1}{\left(1 - \left(|V|/V_b\right)^n\right)}, \tag{2}$$

where $I_{sc}$, $I_0$, $m$ and $V_t$ have their usual meanings, $V_b$ is breakdown voltage and $n$ is the Miller exponent.

In the case of B-type cells, the equation used by the authors is

$$I = I_{sc} - I_0\left(\exp\frac{V}{mV_t} - 1\right) - \frac{V}{R_{sh}}, \tag{3}$$

where $R_{sh}$ is shunt resistance.

This classification between A and B types of reverse characteristic of photovoltaic cells is the same adopted in the international standards IEC-61215 [32] and IEC-61646 [33].

- Later in 1986 Lopez Pineda [34] makes a distinction among three types of reverse $I$–$V$ characteristics depending if the main effect is a low shunt resistance (type-I and type-II curves) or avalanche multiplication (type-III curves). Differences among the three types of reverse characteristics can be appreciated in Fig. 1. The equation is similar to Abergamo's, but written in a unique formula:

$$I = \left(I_{sc} - I_0\left(\exp\frac{V}{mV_t} - 1\right)\right)M(V) - \frac{V}{R_{sh}}, \tag{4}$$

where $M(V)$ is the same expression than in Eq. (2) with the condition that if $V>0 \Rightarrow M(V)=1$, if $V<0 \Rightarrow M(V)>1$ and if $V=V_b$ multiplication coefficient $M(V)$ is infinite ($M(V)=\infty$).

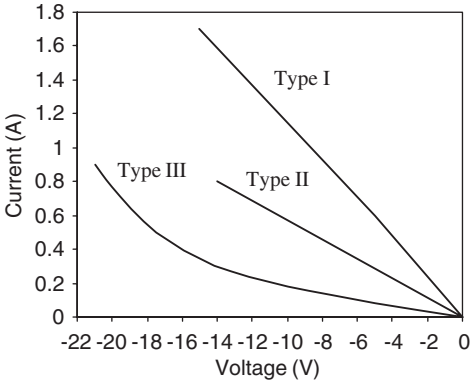


Fig. 1. Different types of reverse bias characteristics in dark conditions according to Pineda.

- Bishop in 1988 [35] proposes an equation in which avalanche breakdown is expressed as a non-linear multiplication factor that affects the shunt resistance term in the one exponential model of the $I-V$ characteristic:

$$I = I_L - I_0\left[\exp\frac{V+IR_s}{mV_t} - 1\right] - \frac{V+IR_s}{R_{sh}}\left[1 + a\left(1 - \frac{V+IR_s}{V_b}\right)^{-n}\right], \qquad (5)$$

where $V_{br}$ is the junction breakdown voltage, and $a$ and $n$ are fitting parameters.

The main difference between Bishop's approach and the rest is that Bishop considers that current components affected by avalanche multiplication are those involved in the shunt resistance term, while in the rest of the approaches primary currents are multiplied (see Fig. 2). From a theoretical point of view, the term of shunt resistance is usually incorporated in solar cell models to simulate complex effects, in general, external to the p–n junction [36]. That means that at least most of its current components should not be affected by avalanche multiplication.

Since the publication of Bishop's model it has been widely used to simulate mismatch effects in different PV solar cell interconnection schemes [37–40]. These works in general use the model to simulate the behaviour of PV arrays from theoretical parameter values taking into account the statistical distribution of them [39,40]. Some of the authors validate the model with experimental measurements on commercial cells calculating unknown parameters by minimization methods [37,38].

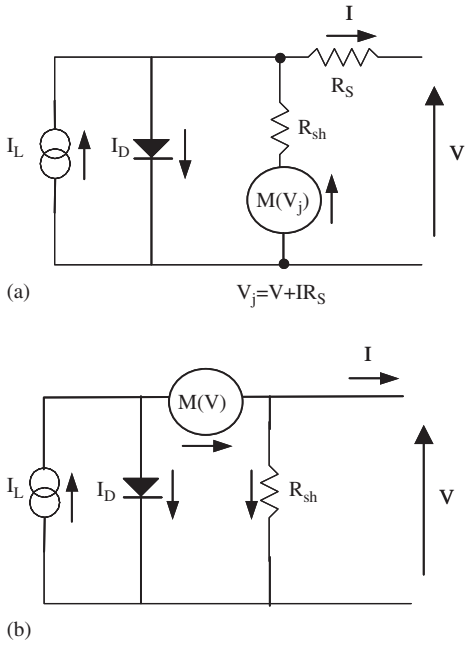


Fig. 2. (a) Reverse bias model electrical schemes according to Bishop, (b) according to other authors.

In a previous phase of this work we have applied the published models to measurements of different photovoltaic cells [41], obtaining good fittings. Nevertheless, there are several drawbacks in current models: First, parameters obtained were in some cases meaningless or out of the range foreseen by theory. For example, the Miller exponent that is included in all models should have values between 3 and 6 according to theory [30], but values found in solar cell measurements are usually out of this range. Furthermore, a fixed value of the $n$ exponent overestimates soft disruption phenomena at low voltages. Besides, the more widespread model does not consider in its formulation the multiplication of primary currents that in our opinion should be considered.

The model used in this paper has been obtained after a detailed study of avalanche mechanisms in PV cells [42] and is a simplified, closed-packed formula of a comprehensive one [43], easy to apply to actual measurements with a procedure briefly outlined in an earlier publication [44]. Development and application of the model has been performed taking into account two objectives:

- Model formulation in keeping with the physical mechanisms that are produced when a commercial photovoltaic solar cell is forced to work in reverse bias.
- Model parameter extraction again coherent with the physical mechanisms and parameter influence areas in order to avoid convergence problems or meaningless parameters that can arise with minimization methods.

## 3. Model development and parameter extraction

### 3.1. Formulation

The proposed model is a closed packed formula of current as a function of voltage expressed as

$$I = \frac{I_N}{1 - K_e} = \frac{I_N}{1 - \exp\left\{B_e\left(1 - \sqrt{(\phi_T - V_b)/(\phi_T - V)}\right)\right\}},$$

$$I_N = a + bV + cV^2 \equiv I_{sc} - G_p V + cV^2 (V \leqslant 0), \tag{6}$$

where $K_e$ is the multiplication coefficient (for electrons), $B_e$ is a non-dimensional cuasi-constant parameter with value [43] $\sim 3$, $V_b$ is breakdown voltage, $\Phi_T$ is the built-in junction voltage (not to be used as an adjustable parameter. For silicon cells of unknown junction structure a typical value, for example, $\Phi_T = 0.85\,V$, should instead be considered).

Numerator of Eq. (6), $I_N$, is a primary effective current. This current could be expressed as a sum of primary currents as they are obtained from the resolution of continuity equations for the solar cell, each one weighted by a multiplication factor that can be obtained taking into account impact ionisation theories [43]. From a practical point of view and to work with experimental data, $I_N$ can be fitted empirically to straight line in which the intercept is the short circuit current $I_{sc}$ and

the slope the shunt conductance $G_p$. This approximation, with the parabolic term $c = 0$, is valid for most dark curves. For illuminated characteristics and those dark curves in which the linear fitting is not sufficient, the addition of the parabolic term $c$ ($c<0$) in $I_N$ adjustment will improve the results. This parameter would comprise different effects related with the way in which primary currents are affected by multiplication factors.

The great variability of reverse $I$–$V$ characteristic of PV cells [20–22,45] has been mentioned in the preceding section, and is widely commented on in the literature. The model proposed in Eq. (6) is valid in cases in which avalanche effects are perceptible in the measurement range. Nevertheless, there are reverse characteristics in which multiplication is not clearly appreciated. This can be due to very high breakdown voltages, unable to be measured under a safe range for the PV cell, or because the reverse characteristic is dominated by the shunt resistance term. In these cases the model is also valid if it little changes in the calculation of the primary current $I_N$ are performed.

### 3.2. Parameter calculation

Parameter calculation has been performed by extracting parameters in those areas of the $I$–$V$ characteristic which are more significant. Hence, $V_b$ is calculated close to the breakdown zone, $I_{sc}$ and $G_p$ in the neighbourhoods of short circuit, and $c$ in the whole characteristic once the other parameters are known. The procedure is described in the following:

#### 3.2.1. Breakdown zone: $V_b$ calculation

Breakdown voltage is calculated by linear regression of the straight line of voltage against the inverse of current. Isolating $V$ in Eq. (6) we have

$$V = V_b + (\Phi_T - V_b)\left[1 - \frac{1}{\left(1 - \left(\ln(1 - I_N/I)/B_e\right)\right)^2}\right]. \tag{7}$$

In the limit, when full breakdown is reached, $I \to \infty$ and $V \to V_b$. After some calculations the following is obtained:

$$V = V_b + \frac{2(\Phi_T - V_b)I_{nb}}{B_e}\frac{1}{I} \equiv V_b + P_b\frac{1}{I} \text{ with } I_{nb} \equiv I_n(V_b). \tag{8}$$

From the intercept of the straight line of $V$ vs. $1/I$ as in Eq. (8), $V_b$ value is obtained. This value can be improved by fitting the function

$$V \approx V_b + P_b f \text{ with } f = \frac{1 - \left[1 - \left(\ln(1 - I_{nb}/I)/B\right)\right]^{-2}}{(2I_{nb}/B)}, \tag{9}$$

where $f$, in the first of the iterations is $1/I$. With the first $P_b$ value $I_{nb}$ is acquired, and then $P_b$, $I_{nb}$ and $f$ function are recalculated. In all practical cases the procedure converges in the first iterations. Fig. 3 schemes the $V_b$ calculation.

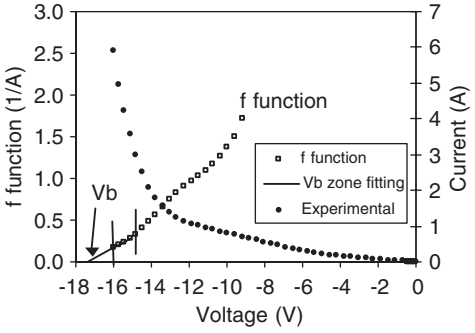


Fig. 3. Procedure for the calculation of breakdown voltage.

*3.2.2. $I_n$ calculation*

With the calculated $V_b$ value, the multiplication coefficient $K_e$ in Eq. (6) is computed using a fixed value of $B_e = 3$. Then $I_N$ is fitted to the straight line:

$$I_N = I(1 - K_e) \equiv I_{sc} - G_p V. \tag{10}$$

If fitting is good and model parameters fall within their appropriate values, the procedure is finished (it is valid in many dark characteristics). In case fitting is not good or parameter values are out of a sensible range, then $I_N$ is fitted to the parabola:

$$I_N = I(1 - K_e) \equiv I_{sc} - G_p V + cV^2. \tag{11}$$

In the present work it has been stressed to procure a general method applicable to different types of reverse characteristics of PV cells, evaluating temperature and irradiance effects, and providing guidelines depending on the shape of the reverse characteristic.

## 4. Samples and experimental details

Reverse bias *I–V* characteristics of different PV cells have been measured. Samples are two c-Si solar cells (denoted S-1 and S-2) with 100 $cm^2$ area, measured at different irradiances and four temperatures (10, 25, 40 and 55 °C). These measurements have been performed indoors with a class A solar simulator in a water controlled thermostatic platform. A limitation in current has been imposed in order to guarantee measurements in a safe range for the cell. Fig. 4 shows an example of the measurements of one of the cells at different irradiances and 55 °C.

In order to cover the different reverse characteristics that can be found within the same cell type, the 33 cells of a commercial m-Si PV module have been measured. The access to the cells have been performed by cutting the tedlar in the rear side of the module and soldering cables to a plug attached in the module frame. In this way

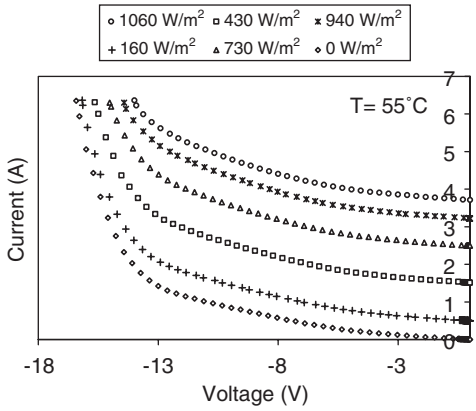


Fig. 4. Reverse bias *I–V* characteristics of sample S-1 measured at different irradiances and 55 °C.

it is possible to measure the cells either individually or associated in strings. Cells are identified as c-1 to c-33.

The measurements of the cells belonging to the module were performed outdoors in a sunny day with stable meteorological conditions, and in dark conditions at ~22 °C. They revealed very different profiles of reverse characteristics, as it is shown in Fig. 5a and b, where some examples of the measured curves are presented in dark conditions (Fig 5a), and under illumination (Fig. 5b). In some of them, for example, curves marked as c-8, c-14 or c-9 in Fig. 5a, it is possible to appreciate the typical knee of the beginning of important avalanche effects, although breakdown voltage appears to be clearly different from one cell to the other. On the other hand, curves marked as c-13, c-28, c-25 and c-10 in Fig. 5-a are examples of a different behaviour. Curve c-28 is dominated by shunt resistance and increases its current very rapidly at low voltages, curve c-13 is very flat in the measurement range and avalanche effects are not easily perceived, and curves c-28 and c-10 are intermediate situations. The same behaviour was found in the measurements of the same cells under illumination, as it can be appreciated in Fig. 5b. The different scale in both graphs has to be noted, corresponding to a shorter voltage measurement range in the illuminated curves to avoid high-power dissipation damaging the cells. This has to be taken into account in the modelling of the characteristic, in order to guarantee a right value of breakdown voltage, as it is to be extracted from regions of the curves close enough to avalanche behaviour.

## 5. Model application

### 5.1. Isolated cells

Measurement conditions, especially temperature and irradiance, are easy to control in isolated cells. These measurements have been used to analyse the influence

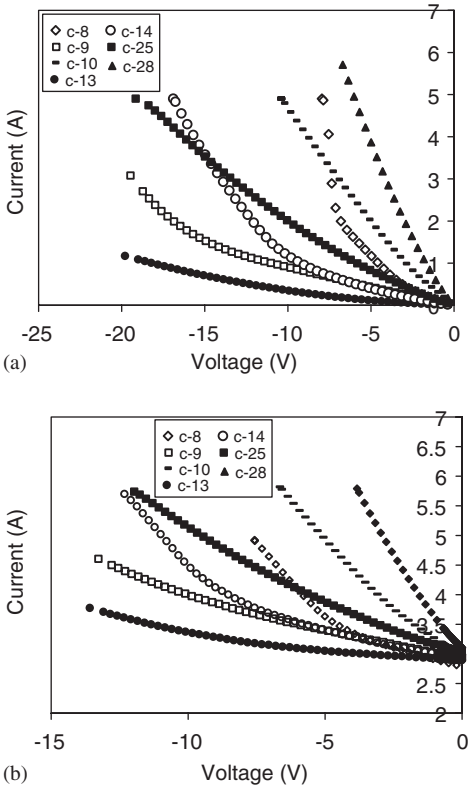


Fig. 5. (a) Reverse bias $I$–$V$ characteristics of different cells belonging to the test module in dark conditions and (b) under illumination. Cells are identified by a number that indicates their position in the module following letter "c".

of both factors, in order to extract conclusions to generalize the calculating parameters procedure.

The application of the proposed model and procedure to measurements at different irradiances revealed that erroneous values can be obtained if breakdown voltages are calculated from regions of the characteristics far from avalanche conditions [44]. For example, Fig. 6 shows the linear fitting for $V_b$ calculation in the farther negative area of two of the characteristics of Fig. 4. It can be observed that the straight line in the measurement at high irradiance does not correspond to the area of intense avalanche, but to an extension of other zones of the characteristic in which other effects may be present. The result is an overestimation in the calculated $V_b$ value.

With these findings it is recommended to obtain breakdown voltage from dark characteristics with enough data points after the knee, indicative of important avalanche effects.

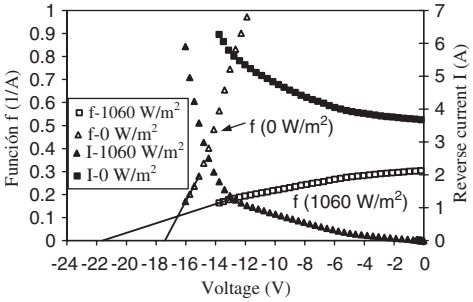


Fig. 6. Breakdown voltage extraction from a reverse $I$–$V$ characteristic measured past the knee of important avalanche (labelled 0 W/m$^2$), and also from another measurement within a shorter measurement range (1060 W/m$^2$). The latter provides an overestimated value of $V_b$.

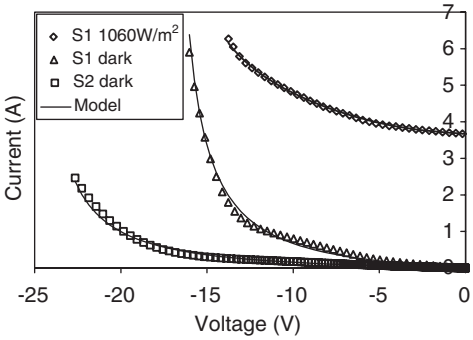


Fig. 7. Experimental and modelled curves of reverse bias measurements in isolated cells.

Table 1
Model parameters corresponding to the curves of Fig. 7

| Sample | $V_b$ (V) | $I_{sc}$ (A) | $G_p$ (A/V) | $c$ (A/V$^2$) | EM (A) | RECM (A) |
|---|---|---|---|---|---|---|
| S1-1060 | −17.4 | 3.66 | 0.04648 | −0.01307 | −0.0024 | 0.027 |
| S1 dark | −17.4 | 0 | 0.04270 | 0 | 0.0055 | 0.067 |
| S2 dark | −25.2 | 0 | 0.01391 | 0 | 0.0046 | 0.093 |

As an example of model application, Fig. 7 shows the experimental and modelled dark curves of two cells, and the experimental and modelled curve under illumination of one of the cells. Model parameters are presented in Table 1, together with the fitting errors calculated as the Mean Error (ME) and Root Mean Squared Error (RMSE). Breakdown voltage in the illuminated curve has been taken as the one calculated from the dark measurement. Primary current $I_N$ has been

adjusted with the linear approximation for dark curves and the parabola for the illuminated one.

### 5.2. Temperature dependence of breakdown voltage

It has been documented that breakdown voltage in p–n junctions can be described according to the relation [46]

$$V_b = V_{b0}(1 + \beta(T - T_0)), \tag{12}$$

where $V_{b0}$ is breakdown voltage at ambient temperature $T_0$ and $\beta$ is breakdown voltage temperature coefficient. Following the cited reference, $\beta$ should be constant with a value of $8.8 \times 10^{-4}\,1/^{\circ}\mathrm{C}$ in a temperature range from 15 to 196 °C. Subsequent studies [47] pointed towards breakdown voltage temperature coefficient as a criteria to distinguish between Zener and avalanche breakdown in silicon p–n junctions. According to this, samples in which $V_b$ has a small value and a negative temperature coefficient are dominated by internal field emission mechanism (Zener), whereas if the predominant mechanism is avalanche the temperature coefficient of breakdown voltage is positive.

Mahedevan et al. [48] accomplished a comprehensive review about electrical breakdown in semiconductors. They collected values of breakdown voltage temperature coefficients in different samples, concluding that for the case of avalanche mechanisms in silicon it ranges between $10^{-4}$ and $10^{-3}\,1/^{\circ}\mathrm{C}$.

There are no specific studies in relation to breakdown voltage variations in silicon solar cells, except the ones presented by Bishop [49]. The author indicates a difference between samples with microplasmas, insensitive to temperature changes, in contrast with samples without microplasmas, highly temperature dependant.

Temperature range used in this work, although not too wide, can be considered common in PV devices. Breakdown voltages obtained with the proposed model and procedure present a clear trend of increase (in absolute values) with the increase of temperature.

A calculation of the temperature coefficient of the obtained breakdown voltages was performed by linear regression. A value of $\beta_{V_b} = 6.031 \times 10^{-4}\,1/^{\circ}\mathrm{C}$ in sample S-1 and $8.638 \times 10^{-4}\,1/^{\circ}\mathrm{C}$ in sample S-2 was found, which is in accordance with theory.

### 5.3. Cells encapsulated in a module

The application of the model to cells belonging to the module has been performed differently depending on the shape of the reverse characteristic. The complete procedure as described in Section 3.2 was applied to those characteristics both in dark and under illumination, in which a clear curvature indicative of avalanche was apparent. In these cases, for the same cell, breakdown voltage was calculated in the dark curve, and applied to the illuminated one.

(a) *Curves with noticeable breakdown zone*: Fig. 8 depicts an example of the application of the complete model and the procedure presented. It presents the experimental and model curves of three cells measured in darkness and at

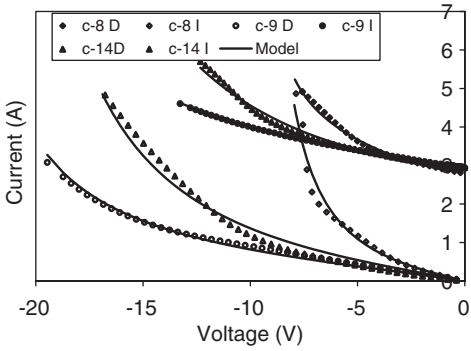


Fig. 8. Experimental and modelled curves of several cells belonging to the test module in which avalanche effects can be appreciated. "D" indicates measurement in dark conditions and "I" under illumination.

Table 2
Model parameters corresponding to the dark curves of Fig. 8

| Cell name | $V_b$ (V) | $I_N = I_{sc} - G_p \times V + c \times V^2$ | | | ME (A) | RMSE (A) |
|---|---|---|---|---|---|---|
| | | $c$ (A/V$^2$) | $G_p$ (A/V) | $I_{sc}$ (A) | | |
| c-8 D | −9.66 | 0 | 0.1400 | | 0.008 | 0.222 |
| c-9 D | −24.41 | −0.00168 | 0.0818 | 0.0 (Darkness) | −0.018 | 0.061 |
| c-14 D | −22.56 | 0 | 0.1034 | | −0.019 | 0.182 |

$\sim$1000 W/m$^2$. Cells are identified by a number, followed by a D indicating a measurement in dark conditions or I indicating a measurement under illumination. It has to be noticed that illuminated characteristics correspond only to a part of their homologous dark curves due to the limitations in current and voltage during the measurement procedure. For this reason breakdown voltage has been obtained from the dark measurement, with more data points close to the breakdown zone. Model parameters and errors when applying the model are presented in Table 2 (dark curves) and Table 3 (under illumination).

(b) *Curves dominated by shunt resistance in the measurement range*: Fig. 9a and b shows an example of model application to characteristics in which the typical knee of the beginning of avalanche is not appreciated. In this case breakdown voltage calculation would render an approximate value, and the procedure shown in previous sections could provide incorrect values. To cope with this difficulty, it was decided to calculate breakdown voltage in these characteristics by minimizing the normal squared distance between the experimental and the modelled curves. Once $V_b$ is calculated, primary current can be fitted. In this point, and given the low sensitivity of the characteristic, a linear fitting for the calculation of $I_N$ is recommended as a first step, passing to the parabolic fit when it is needed. In the examples shown in Fig. 9a and b, all the characteristics have been fitted with the linear approximation

Table 3
Model parameters corresponding to curves under illumination in Fig. 8

| Cell name | $E$ (W/m$^2$) | $T$ (°C) | $V_b$ (V) | $I = I_{sc}$-$G_p \times V + c \times V^2$ | | | ME (A) | RMSE (A) |
|---|---|---|---|---|---|---|---|---|
| | | | | $c$ (A/V$^2$) | $G_p$ (A/V) | $I_{sc}$ (A) | | |
| c-8 I | 859 | 50 | −9.66 | −0.03403 | 0.07861 | 2.81 | −0.0172 | 0.0519 |
| c-9 I | 994 | 30 | −24.41 | −0.00718 | 0.09597 | 2.93 | −0.0045 | 0.0128 |
| c-14 I | 1016 | 30 | −22.56 | −0.00211 | 0.07091 | 2.95 | 0.0071 | 0.0586 |

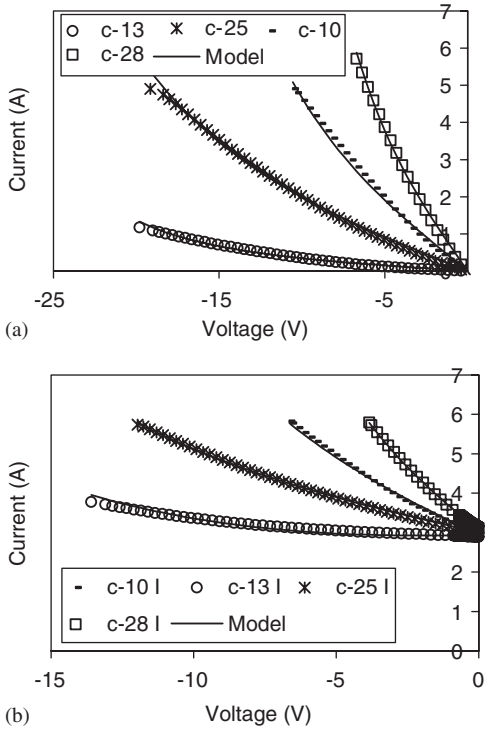


Fig. 9. Experimental and modelled curves of some cells belonging to the test module in which avalanche effects are not easily appreciated in the measurement range. (a) Dark conditions, (b) under illumination.

for $I_N$ except the one noted as c-13 I, in which the parabolic approximation has been performed. Model parameters and errors are presented in Table 4.

## 6. Conclusions

After a critical review of models for reverse $I$–$V$ characteristics of PV solar cells a model and a parameter calculation procedure is proposed. The model, with

Table 4
Model parameters corresponding to the curves of Fig. 9a and b

| Cell name | Model parameters | | | | ME (A) | RMSE (A) |
|---|---|---|---|---|---|---|
| | $V_b$ (V) | $G_p$ (A/V) | $I_{sc}$ (A) | $c$ (A/V$^2$) | | |
| c-10 D | −23.87 | 0.3652 | | 0 | 0.0225 | 0.095 |
| c-13 D | −28.52 | 0.0294 | 0.0 | 0 | 0.0057 | 0.036 |
| c-25 D | −35.64 | 0.1826 | (darkness) | 0 | 0.033 | 0.093 |
| c-28 D | −14.83 | 0.6447 | | 0 | 0.0189 | 0.079 |
| c-10 I | −23.87 | 0.3516 | 2.94 | 0 | −0.0002 | 0.034 |
| c-13 I | −28.52 | 0.0316 | 2.90 | −0.00331 | −0.0016 | 0.050 |
| c-25 I | −35.64 | 0.1701 | 3.00 | 0 | −0.0039 | 0.015 |
| c- 28 I | −14.83 | 0.5843 | 3.06 | 0 | −0.0000 | 0.021 |

physically meaningful parameters, is valid for reverse bias $I$–$V$ characteristics measured at different irradiances and temperatures. It can also be applied to the different types of reverse characteristics found in PV solar cells: those dominated by avalanche mechanisms, and also those in which avalanche is not perceived because they are dominated by shunt resistance or because breakdown takes place out of a safe measurement range. Temperature dependence of breakdown voltage in measured PV cells is in agreement with p–n junctions avalanche theories.

## References

[1] F.A. Blake, K.L. Hanson, The hot-spot failure mode for solar arrays, in: Proceedings of the Fourth Intersociety Energy Conversion Engineering Conference (IECEC), August 1969, pp. 575–581.
[2] P.L. Jett, J.L. Miller, Analysis of effects of shadowed and open solar cells on orbital workshop solar cell array performance, in: Proceedings of the Sixth Intersociety Energy Conversion Engineering Conference (IECEC), August 1971, pp. 889–900.
[3] N.R. Garner. Statistical analysis applied to solar cell shorting caused by reverse bias voltage stress, in: Proceedings of the Ninth IEEE Photovoltaic Specialists Conference, 1972, pp. 142–145.
[4] H.S. Rauschenbach, E.E. Maiden, Breakdown phenomena in reverse biased silicon solar cells, in: Proceedings of the Ninth IEEE Photovoltaic Specialists Conference, Silver Springs, FL, 1972, pp. 217–225.
[5] J.C. Arnett, G.C. González, Photovoltaic module hot spot durability design and test methods, in: Proceedings of the 15th IEEE Photovoltaic Specialists Conference, 1981, pp. 1099–1105.
[6] J.A. Roger, S. Massad, J. Posbic, J. Pivot, Disequilibriums in series conected solar cells, in: Proceedings of the Fourth EC Photovoltaic Solar Energy Conference, 1992, pp. 301–306.
[7] S. Pace, J. Bishop, M. Magni, Hot spot in solar cells. Test procedures and study of related phenomena, in: Proceedings of the Sixth Commission of the European Communities Conference on PV Solar Energy, London, 1986, p. 304.
[8] A. Abete, F. Cane, C. Rizzitano, M. Tarantino, R. Tommasini, Performance testing procedures for photovoltaic modules in mistmatching conditions, in: Proceedings of the 22nd IEEE Photovoltaic Specialists Conference, 1991, pp. 807–811.
[9] A.M. Ricaud, Solar cells failure modes and improvement of reverse characteristics, in: Proceedings of the Fourth EC Photovoltaic Solar Energy Conference, 1982, pp. 392–398.

[10] A.M. Ricaud, F. Forge, P.E. Sarre, Solar cells failure mode under reverse voltages and reliability, in: Proceedings of the 15th IEEE Photovoltaic Specialists Conference, 1981, pp. 1117–1121.
[11] M.S. Swaleh, M.A. Green, Sol. Cells 5 (1982) 183.
[12] A. Gupta, A.G. Milnes, Effects of shading and defects in solar cell arrays: a simple approach, in: Proceedings of the 15th IEEE Photovoltaic Specialists Conference, 1981, pp. 1111–1116.
[13] H.S. Rauschenbach, IEEE Trans. Electron. Devices ED-18 (8) (1971) 483.
[14] N.F. Shepard Jr., R.S. Sugimura, The integration of bypass diodes with terrestrial photovoltaic modules and arrays, in: Proceedings of the 17th IEEE Photovoltaic Specialists Conference, 1984, pp. 676–681.
[15] M. Giuliano, D. Starley, D. Warfield, T. Schuyler, By-pass diode design, application and reliability studies for solar cell arrays, in: Proceedings of the 15th IEEE Photovoltaic Specialists Conference, 1981, pp. 997–1000.
[16] N.A. Al-Rabi, M.M. Al-Kaisi, D.J. Asfer, Sol. Energy Mater. Sol. Cells 31 (1994) 469.
[17] E. Suryanto Hasym, S.R. Wenham, M.A. Green, Sol. Cells 19 (1986–1987) 109.
[18] H. Yoshioka, S. Nishikawa, S. Nakajima, M. Asai, S. Takeoka, T. Matsutani, A. Suzuki, Non hot-spot PV module using solar cells with bypass diode function, in: Proceedings of the 25th IEEE Photovoltaic Specialists Conference, 1996, pp. 1271–1274.
[19] Trends in Photovoltaic Applications, Survey report of selected IEA countries between 1992 and 2003, Report IEA-PVPS T1-13, 2004.
[20] M. Danner, K. Bücher, Reverse characteristic of commercial silicon solar cells—impact on hot spot temperatures and module integrity, in: Proceedings of the 26th IEEE Photovoltaic Specialists Conference, 1997, pp. 1137–1140.
[21] W. Herrmann, W. Wiesner, W. Waassen, Hot spots investigations on PV modules—new concepts for a test standard and consequences for module design with respect to by-pass diodes, in: Proceedings of the 26th IEEE Photovoltaic Specialists Conference, 1997, pp. 1129–1132.
[22] W. Herrmann, M. Adrian, W. Wiesner, Operational behaviour of commercial solar cells under reverse biased conditions, in: Proceedings of the Second World Conference on Photovoltaic Solar Energy Conversion, 1998, pp. 2357–2359.
[23] W. Herrmann, M.C. Alonso, W. Boehmer, K. Wambach, Efective hot-spot protection of PV modules—characteristics of crystalline silicon cells and consequences for cell production, in: Proceedings of the 17th European Photovoltaic Solar Energy Conference, 2001, pp. 1646–1649.
[24] M.C. Alonso, W. Herrmann, R. German, W. Boehmer, K. Wambach, Outdoor hot-spot investigations in crystalline silicon solar modules, in: Proceedings of the 17th European Photovoltaic Solar Energy Conference, 2001, pp. 638–641.
[25] M. Klenk, S. Keller, L. Weber, C. Marckmann, A. Boueke, H. Nussbaumer, P. Fath, R. Burkhart, Investigation of the hot-spot behaviour and formation in crystalline silicon POWER cells, in: Proceedings of the Conference: PV in Europe—From PV Technologies to Energy Solutions, Rome, 2002, pp. 788–791.
[26] M.C. Alonso, W. Herrmann, W. Böhmer, B. Proisy, Prog. Photovolt. Res. Appl. 11 (2003) 293.
[27] D.L. King, B.R. Hansen, J.M. Moore, D.J. Aiken, New methods for measuring performance of monolithic multi-junction solar cells, in: Proceedings of the 28th IEEE Photovoltaic Specialists Conference, 2000, pp. 1197–1201.
[28] F.J. Vorster, E.E. Van Dyk, Prog. Photovolt. Res. Appl. 13 (2005) 55.
[29] R.A. Hartman, J.L. Prince, J.W. Lathrop, Second quadrant effect in silicon solar cells, in: Proceedings of the 14th IEEE Photovoltaic Specialists Conference, San Diego, 1980, pp. 119–122.
[30] S.L. Miller, Phys. Rev. 105 (1957) 1246.
[31] P. Spirito, V. Abergamo, Reverse bias power dissipation of shadowed or faulty cells in different array configurations, in: Proceedings of the Fourth European Photovoltaic Solar Energy Conference, 1982, pp. 296–300.
[32] International Standard IEC-61215:1993, Crystalline silicon terrestrial photovoltaic (PV) modules—design qualification and type approval.
[33] International Standard IEC-61646:1996, Thin-film terrestrial photovoltaic (PV) modules—design qualification and type approval.

[34] C.F. Lopez Pineda, Solid Wind Technol. 3 (2) (1986) 85.
[35] J.W. Bishop, Sol. Cells 25 (1988) 73.
[36] M. Wolf, H. Rauschenbach, Adv. Energy Convers. 3 (1963) 455.
[37] V. Quaschingn, R. Hanitsch, Sol. Energy 56 (6) (1996) 513.
[38] A. Kovach, J. Schmid, Sol. Energy 57 (2) (1996) 117.
[39] D.L. King, J.K. Dudley, W.E. Boyson, PVSIM: a simulation program for photovoltaic modules, cells and arrays, in: Proceedings of the 25th IEEE Photovoltaic Specialists Conference, 1996, pp. 1295–1297.
[40] F. Iannonne, G. Noviello, A. Sarno, Sol. Energy 62 (2) (1998) 85.
[41] M.C. Alonso García, F. Chenlo, Experimental study of reverse biased silicon solar cells, in: Proceedings of the Second World Conference and Exhibition on Photovoltaic Solar Energy Conversion, 1998, pp. 2376–2379.
[42] M.C. Alonso García, Caracterización y modelado de asociaciones de dispositivos fotovoltaicos, Ph.D. Thesis, 2004.
[43] J.M. Ruiz, M.C. Alonso-García., Current multiplication in reverse biased silicon solar cells, in: Proceedings of the 19th European Photovoltaic Solar Energy Conference and Exhibition, 2004, pp. 340–343.
[44] M.C. Alonso-García, J.M. Ruiz, A new model for the characterisation of *I–V* curves of silicon solar cells in reverse bias, in: Proceedings of the 19th European Photovoltaic Solar Energy Conference and Exhibition, 2004, pp. 2607–2610.
[45] TÜV Immissionsschutz und Energiesysteme GMBH (Eds.), Proceedings of IMOTHEE Project Workshop, Cologne, 2002.
[46] K.G. McKay, Phys. Rev. 94 (4) (1954) 877.
[47] M. Singh Tyagi, Solid State Electron. 11 (1968) 117.
[48] Sudha Mahadevan, S.M. Hardas, G. Suryan, Phys. Stat. Sol. (a) S (1971) 335.
[49] J.W. Bishop, Sol. Cells 26 (1989) 335.